Acta Crystallographica Section B
Structural Science
ISSN 0108-7681

Accurate charge density of the tripeptide Ala-Pro-Ala with the maximum entropy method (MEM): influence of data resolution

Andreas Hofmann,[a] Roman Kalinowski,[b] Peter Luger[b] and Sander van Smaalen[a]*

[a]Laboratory of Crystallography, University of Bayreuth, Universitatstrasse 30, D-95440 Bayreuth, Germany, and [b]Institute for Chemistry, Freie University of Berlin, D-14195 Berlin, Germany

Correspondence e-mail: smash@uni-bayreuth.de

Received 15 February 2007
Accepted 17 June 2007

The accurate electron density of Ala-Pro-Ala is determined by the maximum entropy method (MEM), employing the same reflection data measured at 100 K which was used for a multipole refinement by Kalinowski *et al.* [(2007), *Acta Cryst.* Accepted for publication]. Properties of the electron density are compared with the corresponding properties of the static electron density from the multipole model and to the dynamic MEM electron density of trialanine at 20 K. It is thus shown that the increased thermal smearing at 100 K leads to lower electron densities in the bond critical points and atomic charges closer to zero for Ala-Pro-Ala than has been obtained for trialanine at 20 K. The influence of the resolution of the data is investigated by a series of MEM calculations. Atomic charges and atomic volumes are found not to depend on the resolution, but the charge density in the BCPs decreases with decreasing resolution of the dataset. The origin of this dependence is found to lie mostly in the more accurate estimate of the atomic displacement parameters (ADPs) for the higher-resolution datasets. If these effects are taken into account, meaningful information on chemical bonding can be obtained with data at a resolution better than $d_{\min} = 0.63$ Å. Alternatively, low-resolution X-ray diffraction data can be used in accurate electron-density studies by the MEM, if another source of accurate values of the ADPs is available, *e.g.* from refinements with multipole parameters from a database of transferable multipole parameters.

1. Introduction

Nowadays, CCD area detectors in combination with synchrotron radiation enable the acquisition of high-resolution [$(\sin\theta/\lambda)_{\max} > 1.0$ Å^{-1}] X-ray diffraction data of well crystallized compounds (Luger *et al.*, 2004, 2005). X-ray diffraction data at this sub-atomic resolution contain information on the non-spherical character of the electron density, which can be extracted by multipole refinements (Lecomte, 1995; Coppens, 1997). Analysis of these accurate electron-density distributions according to Bader's atoms in molecules (AIM) theory leads to quantitative information on the properties of the atoms, chemical bonds and nonbonding interactions; it also provides a surface for chemical reactivity (Bader, 1990). This kind of information is useful in medicinal chemistry, where a thorough understanding of host–guest relations can be helpful in understanding biochemical reactions and in the process of drug design. Biomolecules like polypeptides and proteins therefore have been the focus of many recent accurate electron-density studies (*e.g.* Jelsch *et al.*, 2000; Li *et al.*, 2002; Checinska *et al.*, 2006; Volkov *et al.*, 2007). Owing to the large number of parameters in such systems, a complete refinement of all the parameters of the classic multipole

© 2007 International Union of Crystallography
Printed in Singapore – all rights reserved

formalism (Hansen & Coppens, 1978) is often not possible due to high correlations between these parameters. The number of independent parameters can be reduced by the use of tabulated multipole parameters, which are then not further refined (Koritsanszky *et al.*, 2002; Lecomte *et al.*, 2004; Dittrich *et al.*, 2005). It has been shown that the extension of the independent spherical-atom model (ISAM) to aspherical atoms with multipole parameters from a databank results in improved descriptions of electron densities in covalent chemical bonds (Jelsch *et al.*, 2000; Dittrich *et al.*, 2005; Volkov *et al.*, 2007). A useful corollary is that more accurate values are obtained for the anisotropic displacement parameters (ADPs). However, the extraction of information beyond established chemical knowledge from accurate electron densities requires the refinement of these densities. Such refinements do not seem feasible for large systems due to the problem of correlated parameters.

The maximum entropy method (MEM; Jaynes, 1957, 1979, 1986) offers an alternative approach to the determination of accurate electron densities which does not suffer from correlated parameters (Sakata & Sato, 1990; Gilmore, 1996). The MEM determines the optimal values of the electron density at the grid points of a grid over the unit cell. Therefore, the resulting electron-density maps are free of restrictions imposed by models and they can reflect any kind electron-density distribution for which evidence is present in the data. The problem with the MEM is that the reconstructed electron density $[\rho^{\rm MEM}(\mathbf{r})]$ may be affected by artefacts such as spurious maxima and ripples (Jauch & Palmer, 1993; Jauch, 1994; de Vries *et al.*, 1996; Roversi *et al.*, 1998; Palatinus & van Smaalen, 2002; Roversi *et al.*, 2002). Within the last several years, improvements have been introduced into the MEM which solve these problems (*e.g.* applying a non-uniform prior and using prior-derived F constraints; de Vries *et al.*, 1996; Iversen *et al.*, 1997; Palatinus & van Smaalen, 2005). Recently we have introduced the use of difference-Fourier maps as the criterion of convergence for the iterations of the MEM (Hofmann *et al.*, 2007). Subsequently we could show that the MEM electron density and the refined multipole model lead to AIM properties of comparable quality in the case of high-resolution, low-temperature (T = 20 K) X-ray diffraction data for the tripeptide trialanine (Hofmann *et al.*, 2007).

However, the eventual aim is to use the MEM for accurate electron-density studies on proteins and large polypetides. According to a search in the protein data bank (http://www.rcsb.org/pdb), X-ray diffraction by protein crystals has been measured at temperatures higher than 20 K in most cases, while data resolutions greater than $d_{\rm min}$ = 0.63 Å are extremely rare (only 4 out of 38 800 entries were found to have such a resolution). The influence of data resolution and higher temperatures (100 K instead of 20 K) on MEM electron-density maps has therefore to be investigated before any accurate electron-density studies with the MEM are attempted on proteins. In the present contribution we report the results of a series of MEM calculations on the tripeptide L-alanyl-L-prolyl-L-alanine (Ala-Pro-Ala). High-resolution X-ray diffraction data measured at T = 100 K have previously been used for a multipole refinement (Kalinowski *et al.*, 2007). Here we analyse and discuss the effect of limited-resolution datasets extracted from the high-resolution data by Kalinowski *et al.* (2007) on the properties of the MEM electron density.

2. The maximum entropy method

The entropy S of a discrete electron density is defined as (Collins, 1982)

$$S = -\sum_{k=1}^{N_p} \rho^k \log\left(\frac{\rho^k}{\rho^k_{\rm prior}}\right), \qquad (1)$$

where the electron-density values ρ^k are defined on a sufficiently fine grid ($N_1 \times N_2 \times N_3 = N_{\rm p}$) over the unit cell, with $\rho^k = \rho(\mathbf{x}_k)$, and $\mathbf{x}_k$ is the position of pixel k. The values of $\rho_{\rm prior}$ define the prior or reference electron density. This is an electron density that is chosen to reflect as much as possible our state of knowledge about the true electron density. The prior is either constant with a value equal to the average electron density, $\rho_{\rm total}/N_{\rm P}$, if no information about the investigated system is available, or it is an educated guess at the electron density, for example, the electron density corresponding to the ISAM refinement (Papoular *et al.*, 2002). MEM electron densities will be closer to the true density if priors are used that are already close to the true density. Experience has shown that a constant prior is insufficient for accurate electron-density studies, while the ISAM prior leads to meaningful results.

According to the maximum entropy principle, the optimal electron density is defined to be the electron density $\{\rho^k\}$ that maximizes the entropy S while fulfilling certain constraints. Besides the normalization of $\{\rho^k\}$

$$C_0 = -1 + \frac{1}{\rho_{\rm total}} \cdot \sum_{k=1}^{N_{\rm P}} \rho^k, \qquad (2)$$

the most important constraint is the so-called F constraint which incorporates the measured structure factors into the maximum entropy calculation

$$C_{\rm F} = -\chi^2_{\rm aim} + \frac{1}{N_{\rm ref}} \sum_{hkl}^{N_{\rm ref}} \left(w_{hkl} \frac{\left|F^{\rm obs}_{hkl} - F^{\rm MEM}_{hkl}\right|^2}{\sigma^2} \right), \qquad (3)$$

where $F^{\rm obs}_{hkl}$ denote the phased observed structure factors of reflections (hkl) and $F^{\rm MEM}_{hkl}$ are the calculated structure factors obtained by the discrete Fourier transform of $\{\rho^k\}$. The w_{hkl} factor represents the various weighting schemes as introduced by de Vries *et al.* (1994). Here we employ weights proportional to the fourth power of the inverse length of the scattering vector. The fourth power, as opposed to other powers of the inverse length of the scattering vector, is equal to the optimal value proposed by de Vries *et al.* (1994). It is also equal to the optimal value that we have established in extensive tests of the effects of using different weights on the results of MEM calculations on trialanine (Hofmann *et al.*, 2007).

The constraints were incorporated into the maximization procedure using the undetermined Lagrange multipliers

Table 1
Summary of crystallographic data (from Kalinowski *et al.*, 2007).

Chemical formula	$C_{11}H_{19}N_3O_4{\cdot}H_2O$
M_r	257.3
Cell setting, space group	Orthorhombic, $P2_12_12_1$
Z	4
T (K)	100
a (Å)	6.825 (1)
b (Å)	9.042 (2)
c (Å)	21.728 (4)
V (Å^3)	1340.9 (5)
Wavelength, λ (Å)	0.56
$(\sin\theta/\lambda)_{max}$ (Å^{-1})	1.4
Completeness (all/obs) (%)	86.2/70.0
R_{int} (all/obs)	0.050/0.030
R_F (multipole)	0.0208
wR_{F^2} (multipole)	0.0261
GoF (multipole)	1.54
Present work	
R_F (ISAM)	0.0352
wR_{F^2} (ISAM)	0.0405
GoF (ISAM)	2.12

method. This leads to a value of zero for the constraints at convergence ($C_0 = C_F = 0$, *i.e.* $\chi^2 = \chi^2_{aim}$). The historical MEM is defined by an F constraint with the value $\chi^2_{aim} = 1.0$ that corresponds to the expectation value of χ^2 as used in the least-squares refinements. Gull (1989) stated that for the MEM a value of $\chi^2_{aim} = 1.0$ is too pessimistic and a value of χ^2_{aim} smaller than 1.0 is desirable. In accordance with this, we have proposed a method based on difference-Fourier maps which determines the optimal value for χ^2_{aim} (Hofmann *et al.*, 2007). The use of the optimal value for χ^2_{aim} appeared to be very important in order to achieve quantitative, reliable, electron-density maps. Theoretically, only values of χ^2_{aim} less than 1 are expected (Gull, 1989; Skilling, 1989), but values larger than 1 can appear if the standard uncertainties of the measured reflection intensities have been estimated to be smaller than their true values.

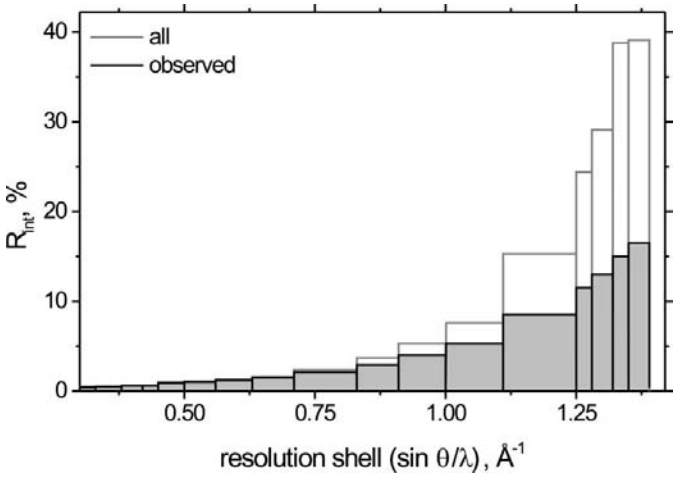

Figure 1
Values of R_{int} for all and the observed reflections in shells of different resolution.

3. Experimental details

3.1. Refinement

Data collection (synchrotron radiation at 100 K) and data reduction have been reported in Kalinowski *et al.* (2007). Fig. 1 shows the internal R value for the different resolution shells of the dataset. The most important crystallographic data are summarized in Table 1. Eight different subsets of the data were created by restricting the resolution to $(\sin\theta/\lambda)_{max} = 0.7$, 0.8, 0.9, 1.0, 1.1, 1.2, 1.3, 1.4 Å^{-1}, respectively. Refinements of the independent spherical atom model (ISAM) were performed for each subset of data with the computer program *JANA*2000 (Petricek *et al.*, 2006). Coordinates from the multipole refinement by Kalinowski *et al.* (2007) have been used as starting positions for all non-H atoms. The C—H bond lengths were fixed to the values known from neutron scattering experiments at low temperatures (Steiner & Saenger, 1993) and an instability factor of 0.01 was used. Final R values smoothly increase with increasing resolution of the dataset (Fig. 2). The crystal structure (obtained by refinement with the

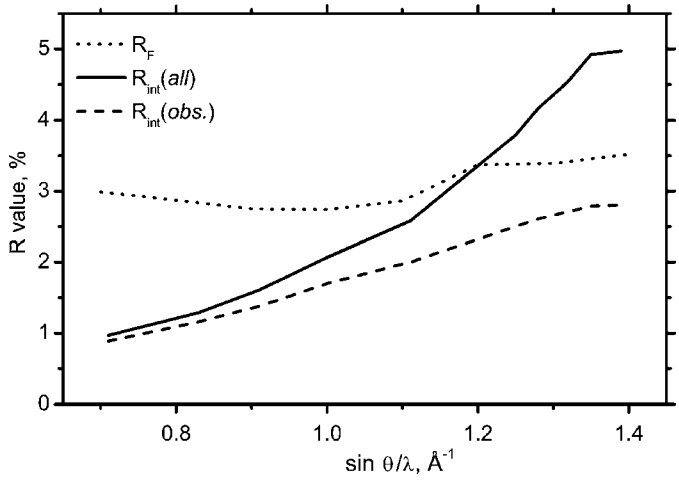

Figure 2
Dependence of R_F (ISAM refinement; dotted line), R_{int} (all data; solid line) and R_{int} (observed data; dashed line) on the resolution of the dataset.

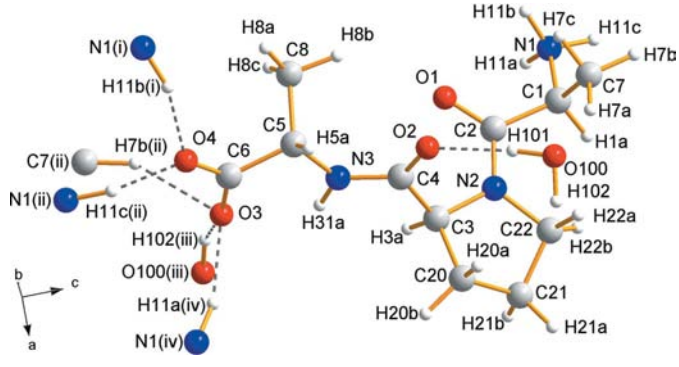

Figure 3
Perspective view of the Ala-Pro-Ala molecule together with the water molecule. The five hydrogen bonds are indicated by dashed lines. Symmetry operations: (i) $-x, -\frac{1}{2}+y, \frac{3}{2}-z$; (ii) $\frac{1}{2}-x, 1-y, -\frac{1}{2}+z$; (iii) $1-x, \frac{1}{2}+y, \frac{3}{2}-z$; (iv) $1-x, -\frac{1}{2}+y, \frac{3}{2}-z$.

Table 2
Averaged atomic charges (integrated number of electrons in an atomic basin minus the corresponding number of protons; first line) and atomic volumes (Å^3; second line: italics).

Note that for $NH_{peptide}$ and NH_3 the contributions of the H atoms could not be separated from the N atom. Therefore, the total charge and total volume for the fragments ($-NH_3$, $-NH-$) are given. Values are given for the prior electron density, various MEM electron densities, the MEM electron density of trialanine (Hofmann *et al.*, 2007) and the static electron density of the multipole model (Kalinowski *et al.* 2007).

	Prior	MEM on a subset of data $\sin\theta/\lambda < 0.8$ Å^{-1}	MEM_{FD}	MEM_{HP}	MEM (trialanine)	Multipole
$NH_{peptide}$	−0.45	−0.51	−0.48	−0.51	−0.5 (1)	−0.52
	16.46	*16.77*	*16.48*	*16.36*	*15 (1)*	*17.35*
$N_{peptide}$	−0.72	−0.70	−0.63	−0.7	–	−0.93
	9.59	*9.45*	*9.15*	*9.23*	–	*10.76*
NH_3	+0.02	+0.13	+0.13	+0.14	+0.40 (5)	+0.61
	23.73	*23.17*	*23.32*	*23.39*	*24 (1)*	*19.52*
$O_{peptide}$	−0.57 (2)	−0.76 (8)	−0.73 (13)	−0.76 (13)	−1.2 (1)	−1.03 (3)
	15.53 (38)	*16.31 (10)*	*16.07 (5)*	*16.23 (7)*	*17 (1)*	*19.07 (59)*
$O_{long\ carboxy}$	−0.65	−0.81	−0.81	−0.84	−1.1 (1)	−1.11
	14.50	*15.25*	*15.20*	*15.44*	*15.8 (2)*	*18.32*
$O_{ahort\ carboxy}$	−0.59	−0.80	−0.83	−0.84	−0.91 (5)	−1.06
	13.45	*14.15*	*14.08*	*13.97*	*16.7 (4)*	*16.86*
$C_{peptide}$	+0.80 (9)	+1.06 (1)	+0.98 (5)	+1.01 (1)	+1.29 (5)	+0.99 (4)
	6.82 (72)	*6.24 (16)*	*6.32 (14)*	*6.19 (1)*	*6.0 (4)*	*6.13 (2)*
$C_{carboxy}$	+0.99	+1.25	+1.19	+1.24	+1.40 (1)	+1.27
	6.38	*5.88*	*6.00*	*6.02*	*6.1 (3)*	*5.80*
C_{alpha}	−0.08 (11)	+0.06 (9)	+0.05 (10)	+0.04 (10)	–	+0.23 (7)
	9.8 (16)	*9.1 (15)*	*9.1 (15)*	*8.9 (15)*	–	*6.84 (18)*
C_{methyl}	−1.08 (11)	−1.05 (6)	−0.94 (1)	*no separation*	–	+0.28 (1)
	18.4 (5)	*16.3 (1)*	*16.1 (4)*	*of C−H possible*	–	*9.40 (2)*
C_{ring}	−0.21 (16)	−0.32 (51)	−0.10 (21)	−0.18 (20)	–	+0.21 (11)
	10.2 (11)	*11.6 (37)*	*9.4 (13)*	*9.53 (99)*	–	*8.21 (18)*

complete dataset) is shown in Fig. 3. Input files for *BAYMEM* (phased reflection data) were created for each subset of data with *JANA*2000, according to the procedure described by Bagautdinov *et al.* (1998). Procrystal priors were computed from the final positional and displacement parameters (anisotropic for C, N, O; isotropic for H) of the ISAM refinements by the module PRIOR of *BAYMEM* (van Smaalen *et al.*, 2003).

3.2. MEM

MEM-optimized electron densities were computed with the latest version of *BAYMEM* (van Smaalen *et al.*, 2003), employing an adapted version of the commercially available *MEMsys*5 algorithm package (Gull & Skilling, 1999). Electron-density maps were analyzed according to Bader's (1990) AIM theory with the module EDMA of *BAYMEM* (van Smaalen *et al.*, 2003). All calculations were performed on a Compaq-DEC ES40 Workstation. For the grid-based MEM the unit cell was divided into 96 × 108 × 256 voxels, corresponding to a voxel edge length of 0.071 × 0.084 × 0.085 Å^3. Reflections with $0.9 < \sin\theta/\lambda < 2.5$ Å^{-1} missing in the data were introduced into the F constraint with structure factors based on the procrystal prior electron density (prior-derived F constraints; Palatinus & van Smaalen, 2005). In the case of the low-resolution subsets of data with $(\sin\theta/\lambda)_{max} = 0.7$ or 0.8 Å^1, prior-derived F constraints were introduced for $0.7 < \sin\theta/\lambda < 2.5$ or $0.8 < \sin\theta/\lambda < 2.5$ Å^{-1}, respectively. The optimal value of $\chi^2_{aim} = 1.30$ was obtained by analysing difference-Fourier maps according to procedures described elsewhere (Hofmann *et al.*, 2007). In order to obtain a better understanding of the influence of the high-angle reflections on the calculated MEM electron density, one additional MEM calculation was performed with a pro-crystal prior based on the positional and displacement parameters obtained from the ISAM refinement with data up to $(\sin\theta/\lambda)_{max} = 1.2$ Å^{-1}, but with a subset of data up to $(\sin\theta/\lambda)_{max} = 0.7$ Å^{-1} in the MEM calculation (extended to a resolution of 2.5 Å^{-1} with prior-derived F constraints). The latter calculation with a high-resolution prior and low-resolution data is denoted by MEM_{HP}; the MEM based on the full dataset is denoted by MEM_{FD}.

4. Results and discussion

4.1. Atom charges and volumes

The MEM is known for its tendency to generate spurious local maxima in electron-density maps (Jauch & Palmer, 1993; Jauch, 1994; de Vries *et al.*, 1996; Roversi *et al.*, 1998; Palatinus & van Smaalen, 2002; Roversi *et al.* 2002). Analysis of the MEM electron densities obtained in the present work shows that atomic maxima are the only local maxima. The volumes of the atomic basins add up to the volume of the unit cell, and the integrated number of electrons is 591.99, *i.e.* only 0.01 electrons less than is obtained from the chemical composition; a difference we attribute to rounding errors. These results show that the measures to suppress artefacts have been successful, in accordance with our results on trialanine (Hofmann *et al.*, 2007).

Owing to its model-independent nature, MEM electron-density maps always represent the distribution of the electron density in the unit cell at the temperature of the measurement. A separation into static structure and effects of thermal motion is not obtained, contrary to the case of multipole refinements. Consequently, topological features are those of dynamical density maps and they are slightly blurred compared with static density maps. Previously we have shown that H atoms do not necessarily constitute local maxima in dynamical density maps, but that they are represented by shoulders on the densities of the atoms to which they are covalently bonded (Hofmann *et al.*, 2007).[1] Accordingly, the atomic basins of H atoms and the bond critical points (BCPs) of $X-H$ bonds are not defined for these H atoms. Instead, the

[1] Notice that this is a property of dynamic densities that is already present in the prior and that it is not a feature generated by the MEM.

analysis according to the AIM theory provides the combined volume (V) and total charge (Q) of a non-H atom X and the H atoms bonded to it. In the present work H atoms bonded to N or O atoms and the atoms H7*b* and H7*c* of the C7 β-carbon methyl group do not constitute local maxima in $\rho^{\rm MEM}(\mathbf{r})$. This effect is found to be dependent on resolution, since in addition the H8*b* and H8*c* atoms do not constitute local maxima in $\rho^{\rm MEM}(r)$ obtained with resolutions of $(\sin\theta/\lambda)_{\rm max} < 1.0$ Å^{-1}. The variation in resolution of the data for the ISAM refinement from 0.7 towards 1.4 Å^{-1} mostly affects the ADP (atomic displacement parameter) values: the higher the resolution, the lower the equivalent isotropic ADPs (Fig. 4). This information is transferred to $\rho^{\rm MEM}(\mathbf{r})$ through the prior electron density. MEM density maps exhibit less pronounced features for datasets of reduced resolutions, apparently resulting in the disappearance of local maxima for H8*b* and H8*c* for resolutions below $(\sin\theta/\lambda)_{\rm max} = 1.0$ Å^{-1}.

The average number of electrons within the atomic basin is +0.2 (2) for those H atoms with a local maximum in $\rho^{\rm MEM}(\mathbf{r})$. This is in agreement with the value of +0.2 (1) for the trialanine (Hofmann *et al.*, 2007), although the spread of values is higher for Ala-Pro-Ala. The integrated number of electrons in the atomic basins of non-H atoms deviates up to 6.9% [average deviation 3.2 (1.9)%] from the values obtained by multipole refinement. Differences between MEM and multipole densities are more pronounced for the ionic charges (integrated number of electrons minus the number of protons of the corresponding atom; Table 2). The two methyl C atoms (C7 and C8) show extraordinary behaviour: the number of electrons deviate by more than 21% from the corresponding multipole values. However, since the multipole results for these methyl groups actually suggest the unlikely situation of a positively charged C atom with three slightly negatively charged H atoms, it is yet to be determined whether the MEM or the multipole values are more accurate.

We could show recently that for a dataset collected at 20 K the atomic charges obtained by the MEM and those obtained by the multipole method agree within standard uncertainties (Hofmann *et al.*, 2007). Larger discrepancies obtained in this study for Ala-Pro-Ala are therefore not a general feature of the MEM, but they can be attributed to the higher temperature of measurement (100 K *versus* 20 K) and the concomitantly larger discrepancies between the dynamic density map at 100 K and the static density map than between the dynamic density at 20 K and the static density. Apart from the charges, large discrepancies are also found for the volumes of the atomic basins, with an average deviation of 16 (13)% for the non-H atoms except C7 and C8, and with a deviation of 68% for the atomic volumes of C7 and C8. It appears that the different sizes of atomic basins in dynamic density maps of different temperatures are a major factor in determining the difference between the integrated number of electrons in these basins.

The influence of the resolution of the dataset on the integrated number of electrons of the non-H atoms is rather small. Different $\rho^{\rm MEM}(\mathbf{r})$ based on the different subsets of the data (§3) exhibit a maximum difference for the integrated number of electrons of 2.4%, which is found for C4. In most cases the difference is much smaller [average value 0.99 (50)%]. The variation is higher in the case of the atomic volumes, with a maximum deviation of 7.8% for C1 [average deviation 2.8 (1.9)%]. Since a systematic dependence on data resolution could not be observed for the atomic volumes and integrated atomic charges, we believe that the observed variations are due to random noise in the data in the different resolution shells. This shows that the integrated atomic charges and volumes which are obtained with MEM are not systematically dependent on the resolution of the data.

4.2. Covalent bonds

Differences between the densities obtained with the MEM and densities corresponding to the ISAM are visualized as difference maps $[\rho^{\rm MEM}(\mathbf{r}) - \rho^{\rm prior}(\mathbf{r})]$. Two-dimensional sections of the difference maps through the peptide bond, *i.e.* sections containing the atoms N2—C2—O1, are shown in Fig. 5 for calculations based on subsets of data at different resolutions. The good quality of the fit to the diffraction data is demonstrated by the absence of features in the corresponding difference-Fourier maps (Figs. 5*b*, *d*, *f* and *h*). The increase in noise in the difference-Fourier maps on increasing the resolution of the data is due to the larger amount of noise in the data at high resolution than is present in the low-resolution data, as becomes apparent from the increase of $R_{\rm int}$ with increasing resolution (Fig. 1). Noise is particularly strong in data with $\sin\theta/\lambda > 1.0$ Å^{-1}. Accordingly, difference maps for $\rho^{\rm MEM}(\mathbf{r})$ and $\rho^{\rm prior}(\mathbf{r})$ generated with these data reflect this noise to some extent: the contour lines of equal density are not as smooth as they are for lower resolutions (Fig. 5).

Despite the increased blurriness due to the relatively high temperature (100 K) of the measurement, all the relevant topological details, such as the charge accumulation in covalent bonds and the lone pairs of the O atom, are displayed properly in difference maps for $\rho^{\rm MEM}(\mathbf{r})$ and $\rho^{\rm prior}(\mathbf{r})$ obtained with the high-resolution subsets of data [$(\sin\theta/\lambda)_{\rm max}$ >

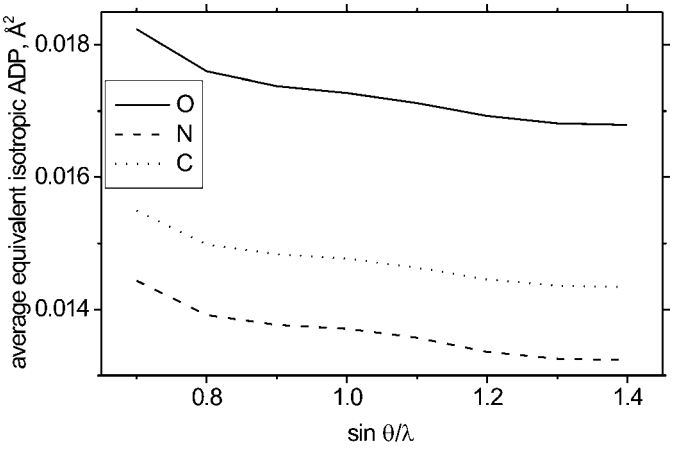

Figure 4
Average equivalent isotropic ADPs for ISAM refinements dependent on the resolution of the data subsets.

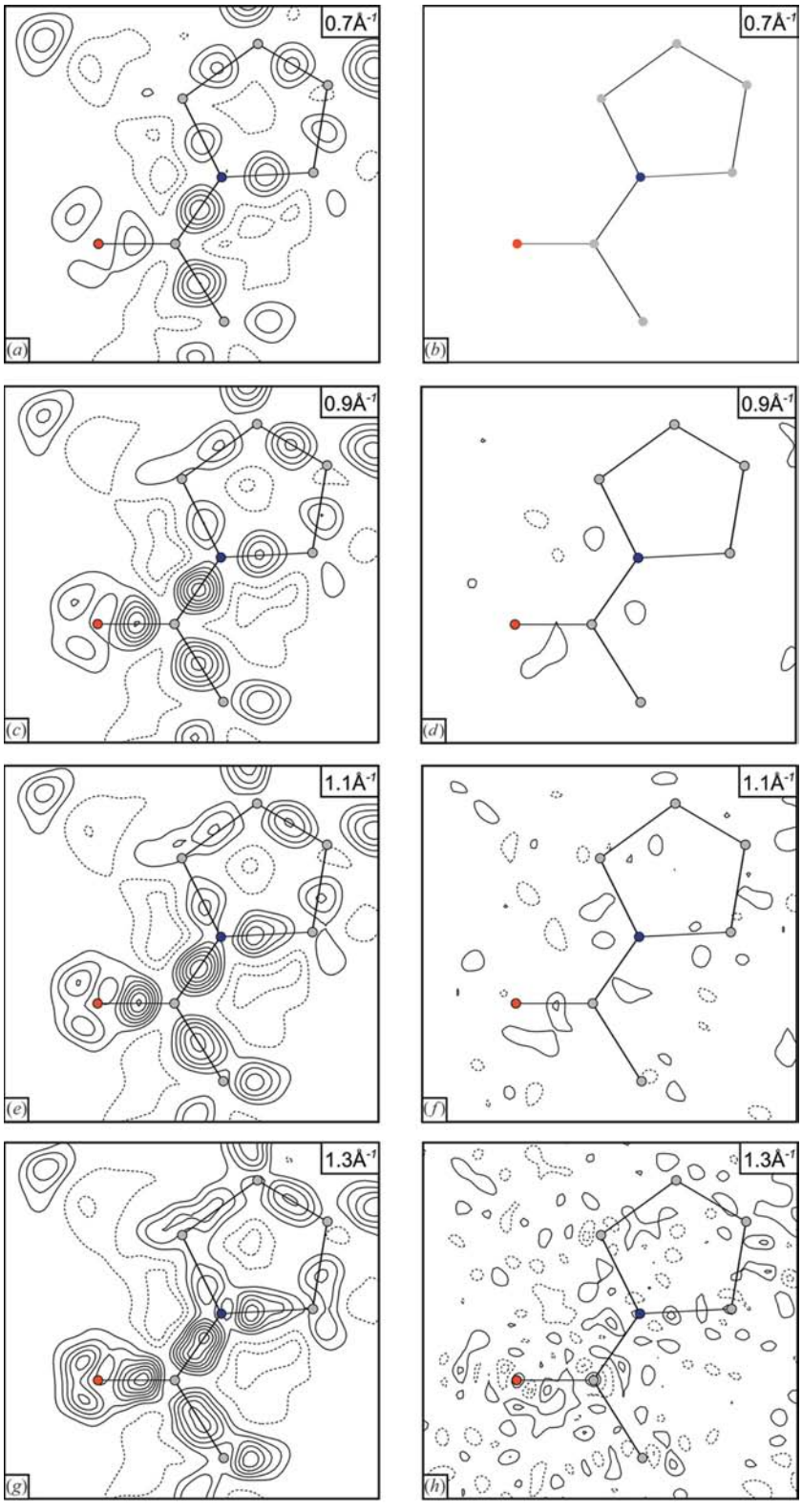

Figure 5
Difference map ($\rho^{MEM} - \rho^{prior}$; *a*, *c*, *e*, *g*) and residual maps (inverse Fourier transformation of $F^{obs} - F^{MEM}$; *b*, *d*, *f*, *h*) of the peptide bond plane N2—C2—O1, for different resolutions of the data subset used in the calculations; the value of $(\sin\theta/\lambda)_{max}$ is indicated. Contour lines are at 0.05 e Å^{-3}.

0.9 Å^{-1}]. However, the difference map which was obtained with data of resolution $(\sin\theta/\lambda)_{max}$ = 0.7 Å^{-1} indicates the lack of certain topological features (Fig. 5*a*). Increasing the resolution of the data has the largest effect on the electron densities in the vicinity of the atomic positions, while its effect on the densities near the BCPs is much smaller (Fig. 6). This qualitative judgement on the basis of visual inspection of the difference maps is supported by a quantitative analysis according to AIM theory. The dependence of the average electron densities in the BCPs on resolution reveals an interesting trend (Fig. 7). Bonds with the lower values of ρ_{BCP} exhibit only a weak dependence of ρ_{BCP} on the resolution of the data: a difference of less than 1.5% between the highest and the lowest value of ρ_{BCP} is observed for the C—C and C_α—N bonds. On the other hand, the electron-rich bonds exhibit a much stronger dependence on the resolution of the data, with an increase of ρ_{BCP} by 6% for the $C_{peptide-Npeptide}$ bond, and by 7% for the C—O bonds, on going from a resolution of 0.7 Å^{-1} towards 1.4 Å^{-1} (Fig. 7). The largest step in ρ_{BCP} is observed for an increase of $(\sin\theta/\lambda)_{max}$ from 0.7 to 0.8 Å^{-1}. The remaining difference in ρ_{BCP} between the electron density MEM_{FD} and the MEM electron density obtained with the subset of data defined by $(\sin\theta/\lambda)_{max}$ = 0.8 Å^{-1} is only 5% for the C—O bonds and less than 3% for the $C_{peptide}$—$N_{peptide}$ bond (Table 3). These results show that high-resolution data are required for an exact description of the electron density in the chemical bond, but they also suggest that meaningful information on certain topological features might already be obtained with data with a resolution of $(\sin\theta/\lambda)_{max}$ = 0.8 Å^{-1} (d_{min} = 0.63 Å). A more detailed analysis of the effects of resolution of the data on the MEM electron densities is given in §4.4.

Electron densities in the BCPs of covalent bonds are 8–19% lower for the MEM electron density obtained with the complete dataset (MEM_{FD}) than for the static electron density obtained from the multipole model. For trialanine, differences of ρ_{BCP} between the dynamic MEM electron density at 20 K and the static electron density from the multipole model have been found to be in the range 1–16%

Table 3
Averaged values of ρ (first line; in e Å^{-3}) and of the Laplacian $\nabla^2\rho$ (second line; in e Å^{-5}; italics) at the BCPs for the different bond types in Ala-Pro-Ala.

Values are given for the prior electron density, various MEM electron densities, the MEM electron density of trialanine (Hofmann *et al.*, 2007) and the static electron density of the multipole model (Kalinowski *et al.* 2007).

	Prior	MEM on a subset of data $\sin\theta/\lambda < 0.8$ Å^{-1}	MEM_{FD}	MEM_{HP}	MEM (trialanine)	Multipole
$C_{peptide}-O_{peptide}$	2.14 (3)	2.37 (1)	2.50 (1)	2.44 (1)	2.55 (2)	2.93 (4)
	27.0 (3)	*27.8 (33)*	*9.8 (90)*	*21.4 (50)*	*23 (9)*	*−31.6 (3)*
$C_{peptide}-N_{peptide}$	1.72	1.98 (4)	2.04 (2)	2.01 (4)	2.18 (5)	2.44 (2)
	3.1	*−5.1 (27)*	*−8.6 (39)*	*−6.2 (21)*	*−17 (4)*	*−22.6 (7)*
Long $C_{carbox}-O$	2.04	2.23	2.36	2.28	2.44 (1)	2.73 (2)
	22.6	*24.2*	*4.9*	*20.8*	*10 (5)*	*−29.2*
Short $C_{carbox}-O$	2.09	2.32	2.43	2.36	2.47 (3)	2.79 (3)
	27.0	*24.6*	*13.5*	*22.6*	*23 (5)*	*−30.0*
$C_{\alpha}-N_{ammonium}$	1.38	1.56	1.57	1.57	1.67 (4)	1.75 (2)
	2.0	*−4.5*	*−4.1*	*−3.4*	*−8 (1)*	*−9.9*
$C_{\alpha}-N_{peptide}$	1.40 (4)	1.56 (6)	1.58 (6)	1.60 (7)	1.74 (1)	1.81 (7)
	1.9 (4)	*−4.5 (4)*	*−3.0 (11)*	*−4.7 (3)*	*−8 (3)*	*−13.4 (37)*
$C_{\alpha}-C_{methyl}$	1.17 (0)	1.36 (1)	1.35 (2)	1.38 (1)	1.48 (2)	1.65 (2)
	−0.2 (1)	*−7.8 (11)*	*−2.1 (22)*	*−7.3 (4)*	*−9 (1)*	*−9.4 (0)*
$C_{\alpha}-C_{peptide}$	1.17 (1)	1.44 (1)	1.42 (2)	1.47 (1)	1.52 (5)	1.75 (1)
	−0.2 (1)	*−9.8 (8)*	*−2.9 (38)*	*−9.1 (10)*	*−7 (3)*	*−11.70 (7)*
$C_{\alpha}-C_{carbox}$	1.14	1.43	1.40	1.46	1.53 (1)	1.72 (1)
	0.0	*−10.6*	*−2.5*	*−10.1*	*−5.4 (3)*	*−12.2*
$C_{ring}-C'_{ring}$	1.18 (1)	1.40 (3)	1.49 (3)	1.41 (2)	–	1.62 (2)
	−0.1 (2)	*−8.7 (4)*	*−6.0 (10)*	*−7.8 (1)*	–	*−9.5 (1.0)*
Ring	0.43	0.35	0.33	0.33	–	0.28
	4.3	*5.2*	*5.6*	*5.0*	–	*4.8*

(Hofmann *et al.*, 2007). In the latter case, the differences have been attributed to the peculiarities of both methods. An estimate of the effect of temperature is therefore best obtained by a comparison between MEM electron densities of Ala-Pro-Ala and those of trialanine. Values of ρ_{BCP} are on average 5.8 (2.9)% smaller for Ala-Pro-Ala than for trialanine electron densities. For the C—O bonds the difference is relatively small (up to 3.3%), while it is higher for C—C and C—N bonds (up to 8.8 and 9.2%, respectively). The reason for this difference lies in the different temperatures of the measurement (100 *versus* 20 K). With increased thermal motion, features become broader and the magnitudes of maxima and minima become smaller. This implies a reduction in the value of ρ_{BCP}, because the BCP is a point where the density has maxima in two directions and a minimum in the third direction. The effect of thermal motion on ρ_{BCP} has not been quantified yet, but calculations with different values for the ADPs have shown that a difference in ρ_{BCP} of up to 3% can be expected if a static electron-density map is compared with a dynamic map measured at 20 K. The observed difference of up to 9.2% therefore seems reasonable if the 20 K data (trialanine) is compared with the 100 K data of Ala-Pro-Ala. Despite the differences between static densities and dynamic electron densities at different temperatures, the general trends of the properties of the densities are the same for different maps: $\rho_{BCP}(C-O_{peptide}) > \rho_{BCP}(C-O_{long\ carboxy}) > \rho_{BCP}(C-O_{short\ carboxy}) > \rho_{BCP}(C_{peptide}-N_{peptide}) > \rho_{BCP}(C_{\alpha}-N_{peptide}) \geq \rho_{BCP}(C_{\alpha}-N_{ammonium}) > \rho_{BCP}(C-C)$. Only within the group of C—C bonds is the sequence different for different maps, but in this case the values of ρ_{BCP} are nearly equal for both MEM (20 and 100 K) and multipole maps. Statistical variations might thus be responsible for these differences.

Thermal motion broadens features corresponding to the maxima and minima in the density maps. Therefore, it decreases the magnitudes of the corresponding curvatures. Since the Laplacian is the sum of the principal values of the curvature in the BCP, its magnitude is strongly affected by the temperature. If all curvatures are affected to the same degree, the algebraic sign remains unchanged, only the absolute value is reduced. This is observed if the Laplacian for the BCPs of Ala-Pro-Ala are compared with the corresponding BCPs in the case of trialanine. The algebraic signs remain untouched, whereas the absolute value of the Laplacian is on average 55 (10)% smaller for Ala-Pro-Ala compared with the values in trialanine.

4.3. Hydrogen bonds

Analysis of the MEM electron densities according to the AIM theory indicates three N—H···O and two O—H···O hydrogen bonds in the asymmetric unit (Fig. 3), in accordance with the results obtained from the multipole density (Kalinowski *et al.*, 2007). The electron density in the BCP increases with decreasing bond length (Table 4) both for the dynamic electron densities and the static density obtained from the multipole model. Magnitudes of ρ_{BCP} are on average 57% higher for MEM_{FD} than for the multipole model, while MEM electron densities of different resolutions and their prior densities led to comparable values of ρ_{BCP} (Table 4). A similar trend was found for trialanine, where the electron densities were on average 49% higher for the MEM than for the multipole refinement (Hofmann *et al.*, 2007). These results suggest that the multipole model might not be able to satisfactorily describe the electron densities in the hydrogen bonds owing to the restrictions on the smooth multipole functions inherent to this model, while the MEM can reproduce any shape of density without being restricted to certain radial functions. This interpretation is in accordance with problems in the description of the electron density around H atoms

Table 4
Values of ρ (first line; in e Å^{-3}) and of the Laplacian $\nabla^2\rho$ (second line; in e Å^{-5}; italics) at the BCPs for the different hydrogen bonds in Ala-Pro-Ala in comparison to the values obtained from the multipole model by Kalinowski *et al.* (2007).

The bond lengths were taken from the ISAM refinement.

			MEM			
	H···O (Å)	Prior	sin θ/λ < 0.8 Å^{-1}	MEM_{FD}	MEM_{HP}	Multipole
O2···H101—O100	1.921 (8)	0.24	0.23	0.23	0.22	0.13 (2)
		1.9	*0.7*	*0.7*	*1.29*	*2.12 (4)*
O3···H102—O100	2.03 (1)	0.20	0.2	0.20	0.20	0.10 (1)
		1.6	*1*	*0.8*	*0.73*	*1.98 (3)*
O3···H11*a*—N1	1.905 (7)	0.26	0.23	0.22	0.22	0.16 (1)
		2.5	*2*	*2.1*	*2.44*	*2.46 (2)*
O4···H11*b*—N1	1.833 (4)	0.29	0.28	0.29	0.28	0.23 (1)
		2.6	*2.4*	*2.2*	*2.46*	*2.06 (2)*
O4···H11*c*—N1	1.795 (4)	0.31	0.32	0.32	0.31	0.22 (2)
		2.8	*2*	*1.7*	*2.56*	*2.27 (3)*

within the multipole model owing to the restrictions imposed by the model parameters (Volkov, Gatti, Abramov & Coppens, 2000; Madsen *et al.*, 2004; Koritsanszky, 2006). This also explains the differences in the Laplacians (Table 4) which are known to depend on the radial functions of the multipole model (Volkov, Abramov, Coppens & Gatti, 2000).

A comparison of the properties of hydrogen bonds between trialanine and Ala-Pro-Ala is not immediately possible, because the two compounds contain hydrogen bonds of different lengths. Furthermore, if the covalent bonds are taken as a guideline, the expected differences would be smaller than 10%, that is ρ_{BCP} would differ by less than 0.035 e Å^{-3}, a value which is close to the noise level. The small values of ρ_{BCP} also complicate the interpretation of the dependence of properties of hydrogen bonds on the resolution of the data. The observed average variation of ρ_{BCP} of 6% between MEM densities based on subsets of data of different resolutions lies below the noise level and cannot be used to determine any particular dependence on the resolution.

4.4. Medium-resolution data cut-off with ADPs from higher-resolution data

This study has shown that the MEM electron density depends to a certain degree on the resolution of the dataset (§§4.1 and 4.2). The bond topology is especially affected, resulting in higher electron densities at the BCP for higher-resolution datasets (Table 3). This is surprising since it is generally accepted that valence electrons, which are responsible for the bond formation, do not significantly contribute to the scattering factors at resolutions higher than sin θ/λ = 0.7 Å^{-1} (Giacovazzo, 1992). However, high-resolution data are necessary for an exact assessment of the anisotropic ADPs which are necessary to separate the bonding contributions from dynamic effects (Jelsch *et al.*, 1998). ADPs are incorporated into the MEM *via* the prior. Therefore, it is interesting to separate the effects of data resolution in the MEM calculation and variations of the values of ADPs with concomitant variations of the prior. For this purpose a MEM calculation was performed with a high-resolution prior and low-resolution data (MEM_{HP}; §3.2).

In general, the topological properties of MEM_{HP} are much closer to the corresponding properties of MEM_{FD} than those of the MEM calculation entirely based on the low-resolution data of $(\sin\theta/\lambda)_{max}$ = 0.7 Å^{-1}. Atomic charges and atomic volumes are comparable for MEM_{HP} and MEM_{FD} (Table 2). The average difference of 2.4 (1.7)% for ρ_{BCP} of the covalent C—C, C—N and C—O bonds between MEM_{HP} and MEM_{FD} is much smaller than the difference between MEM_{FD} and the MEM calculations entirely based on low-resolution data (Table 3). Surprisingly the C—C bonds here show the highest difference (up to 5.4%), although they showed the least

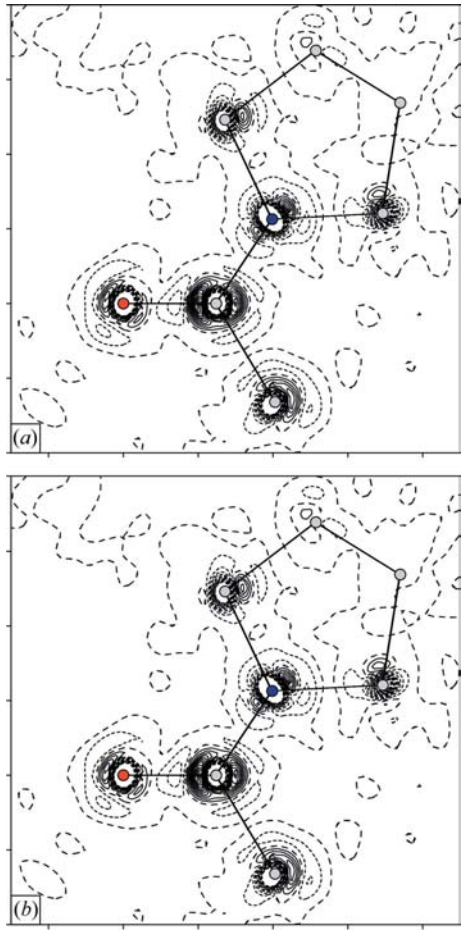

Figure 6
Differences between $\rho^{MEM}(\mathbf{r})$ obtained at various resolutions of the datasets. (*a*) ρ^{MEM} (resolution = 0.8 Å^{-1}) − ρ^{MEM} (resolution = 1.2 Å^{-1}); maximum/minimum differences are 0.68/−2.48 e Å^{-3}. (*b*) ρ^{MEM}(resolution = 0.9 Å^{-1}) − ρ^{MEM} (resolution = 1.2 Å^{-1}); maximum/minimum differences are 0.32/−1.99 e Å^{-3}. Contour lines at 0.05 e Å^{-3}; dashed contours for negative differences; the zero contour is displayed as long dashed curves.

dependence on resolution when employing MEM calculations entirely based on low-resolution data (§4.2). Laplacians are sometimes more positive and in other cases more negative for MEM_{HP} than they are for MEM_{FD}. Despite difference values of up to 16 e Å^{-5}, differences between MEM_{HP} and MEM_{FD} are still smaller than in cases where the high-resolution prior is not used (up to 27 e Å^{-5} in the latter case).

The good agreement between electron-density maps is also reflected in the flat-difference map for MEM_{FD} and MEM_{HP} (Fig. 8). Of course, MEM_{HP} produces a smoother map than MEM_{FD}, since its calculation is not exposed to the high levels of noise of the data at higher resolutions. Observed differences are still small (less than 0.1 e Å^{-3}) and they are located close to the atomic positions, where the influence of the core electrons, which contribute to high-resolution scattering factors, is high. The calculation of MEM_{HP} shows that an electron-density distribution of reasonable quality can be obtained when the MEM is applied to low-resolution datasets, if a reasonably accurate estimate of the ADPs is available. The latter can be obtained, for example, from refinements employing multipole parameters from a database of transferable multipole parameters (Jelsch *et al.*, 2000; Dittrich *et al.*, 2005; Volkov *et al.*, 2007).

5. Conclusions

An accurate electron density of the tripeptide Ala-Pro-Ala has been obtained with the MEM applied to high-resolution X-ray diffraction data measured at $T = 100$ K by Kalinowski *et al.* (2007). In a previous publication we introduced a method for the determination of the point of convergence of the MEM, which is based on the analysis of difference-Fourier maps (Hofmann *et al.*, 2007). This method also proved to be successful for the present calculations. The resulting optimum value of 1.30 for χ^2_{aim} [see (3)] is larger than allowed by theory and thus suggests that the standard uncertainties of the dataset have been estimated with values which are systematically too small. This interpretation is supported by the values of the goodness-of-fit (GoF) for the multipole refinements of Ala-Pro-Ala and trianaline (Rödel *et al.*, 2006). For Ala-Pro-Ala the GoF is 1.54 and $\chi^2_{aim} = 1.30$ (Table 1), while for trialanine the GoF is 0.67 and $\chi^2_{aim} = 0.43$. In both cases χ^2_{aim} is smaller

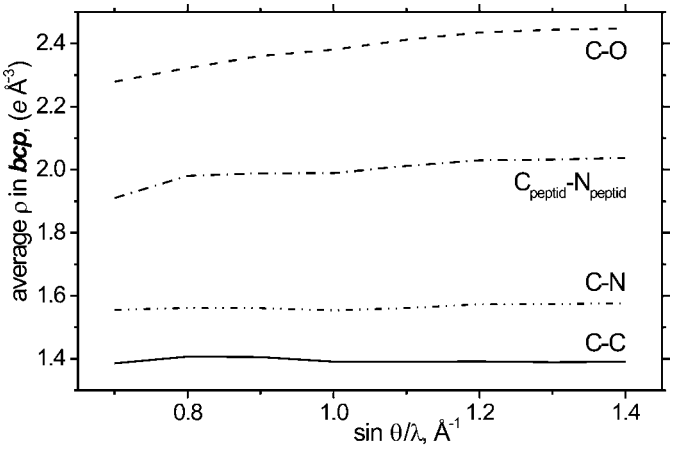

Figure 7
Average electron densities in the BCPs for different types of bonds dependent on the resolution of the data subset.

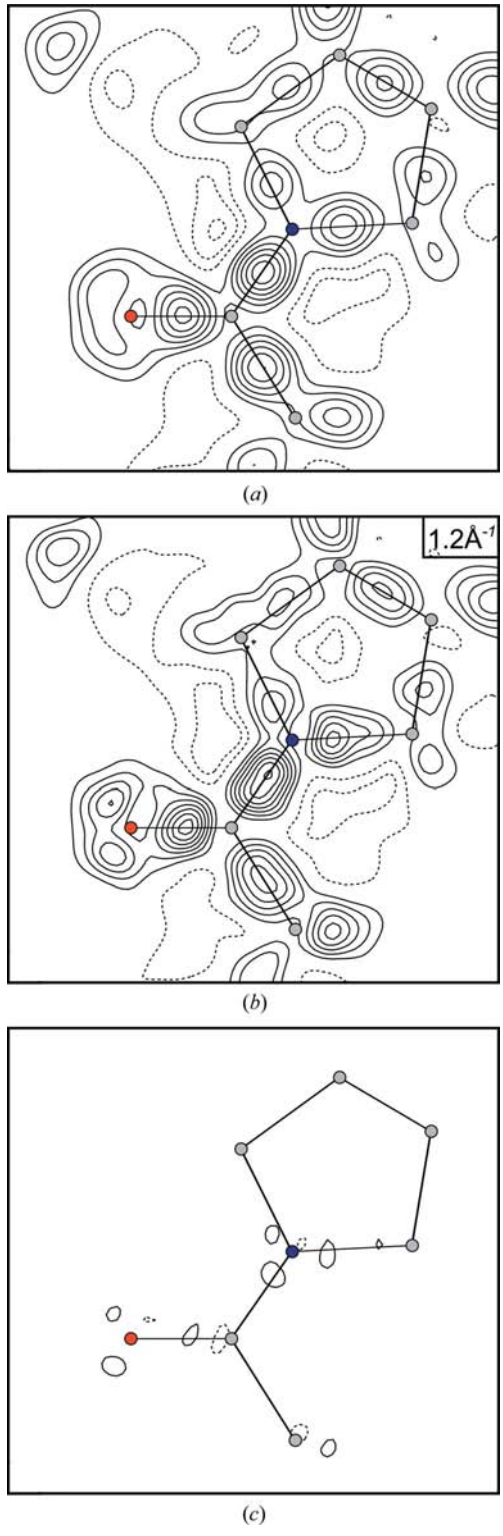

Figure 8
(*a*) $\rho^{MEM} - \rho^{prior}$ for MEM_{HP} (§§3.2 and 4.4); (*b*) $\rho^{MEM} - \rho^{prior}$ for the resolution $(\sin\theta/\lambda)_{max} = 1.2$ Å^{-1} for the data subset; (*c*) difference map $\rho^{MEM}(a) - \rho^{MEM}(b)$.

than the GoF by 0.24, thus indicating for both datasets that the MEM leads to a fit which is closer to the data than the multipole refinements, as required by theory (Gull, 1989), while the standard uncertainties of the trialanine data are probably larger than their true values.

MEM electron densities are dynamic electron densities as opposed to the static electron densities that are usually analysed for multipole models. The relatively high temperature of measurement (100 K) is responsible for a more diffuse character of the MEM electron density of Ala-Pro-Ala compared with the MEM electron density of trialanine at 20 K. The atomic charges (integrated number of electrons minus the nuclear charge) are closer to zero for Ala-Pro-Ala than for trialanine (Table 2), and $\rho_{\rm BCP}$ for covalent bonds is slightly smaller for Ala-Pro-Ala (Table 3). The values of the Laplacians in the BCPs vary over a much greater range, in agreement with the properties of the second derivatives of electron densities which are strongly dependent on the details of the density. In general, the properties of the MEM electron density of trialanine at 20 K are closer to the corresponding static electron density of the multipole model than is the case for the MEM electron density of Ala-Pro-Ala at 100 K.

A series of MEM calculations have been performed with subsets of data with resolutions between 0.7 and 1.4 Å^{-1} for $(\sin\theta/\lambda)_{\rm max}$. Atomic volumes and charges do not depend on the resolution, but $\rho_{\rm BCP}$ is found to increase with increasing resolution of the data (Fig. 7). It has been shown that the dependence of $\rho^{\rm MEM}(\mathbf{r})$ on the resolution lies mostly on the better estimates of ADPs for data of higher resolution (Fig. 4), which enter the MEM through the prior (see §4.4). If a better estimate of ADPs is available than can be obtained with the ISAM refinement (*e.g.* from a refinement with multipole parameters from a database of transferable multipole parameters), it is possible to obtain accurate electron-density distributions with the MEM applied to low-resolution data.

Apart from the problems with $\rho^{\rm MEM}(\mathbf{r})$ based on datasets of reduced resolutions, we have shown that a meaningful $\rho^{\rm MEM}(\mathbf{r})$ value can be obtained on the basis of data with $(\sin\theta/\lambda)_{\rm max} = 0.8$ Å^{-1}. Atomic charges and atomic volumes are well reproduced, while $\rho_{\rm BCP}$ is systematically underestimated for the reduced dataset. With these limitations it is possible to apply the MEM to studies of accurate electron densities of proteins with datasets of resolutions better than $(\sin\theta/\lambda)_{\rm max} = 0.8$ Å^{-1} ($d_{\rm min} = 0.63$ Å). Data of this quality is presently available for a few proteins. It is likely that future developments in protein diffraction, including experiments at 20 K, will allow us to collect data with a resolution greater than 0.63 Å for many more protein crystals.

Financial support was obtained from the German Science Foundation (DFG) within the framework of SPP1178.

References

Bader, R. F. W. (1990). *Atoms in Molecules: a Quantum Theory*. Oxford: Clarendon Press.

Bagautdinov, B., Luedecke, J., Schneider, M. & van Smaalen, S. (1998). *Acta Cryst.* B**54**, 626–634.

Checinska, L., Förster, D., Morgenroth, W. & Luger, P. (2006). *Acta Cryst.* C**62**, o454–o457.

Collins, D. M. (1982). *Nature*, **298**, 49–51.

Coppens, P. (1997). *X-ray Electron Densities and Chemical Bonding*. Oxford University Press.

Dittrich, B., Hübschle, C. B., Messerschmidt, M., Kalinowski, R., Girnt, D. & Luger, P. (2005). *Acta Cryst.* A**61**, 314–320.

Gilmore, C. J. (1996). *Acta Cryst.* A**52**, 561–589.

Giacovazzo, C. (1992). *Fundamentals of Crystallography*, edited by C. Giacovazzo, pp. 141–228. Oxford University Press.

Gull, S. F. (1989). *In Maximum Entropy and Bayesian Methods*, edited by J. Skilling, pp. 53–71. Dordrecht: Kluwer Academic Publishers.

Gull, S. F. & Skilling, J. (1999). *Quantified Maximum Entropy. MemSys5 User's Manual.* Bury St. Edmunds, Suffolk, England.

Hofmann, A., Netzel, J. & van Smaalen, S. (2007). *Acta Cryst.* B**63**, 285–295.

Hansen, N. K. & Coppens, P. (1978). *Acta Cryst.* A**34**, 909–921.

Iversen, B. B., Jensen, J. L. & Danielsen, J. (1997). *Acta Cryst.* A**53**, 376–387.

Jauch, W. (1994). *Acta Cryst.* A**50**, 650–652.

Jauch, W. & Palmer, A. (1993). *Acta Cryst.* A**49**, 590–591.

Jaynes, E. T. (1957). *Phys. Rev.* **106**, 620–630.

Jaynes, E. T. (1979). *The Maximum Entropy Formalism*, edited by R. D. Levine & M. Tribus, pp. 15–118. Cambridge: MIT Press.

Jaynes, E. T. (1986). *Maximum Entropy and Bayesian Methods in Applied Statistics*, edited by J. H. Justice, pp. 26–58. Cambridge University Press.

Jelsch, C., Pichon-Pesme, V., Lecomte, C. & Aubry, A. (1998). *Acta Cryst.* D**54**, 1306–1318.

Jelsch, C., Teeter, M. M., Lamzin, V., Pichon-Pesme, V., Blessing, R. H. & Lecomte, C. (2000). *Proc. Natl. Acad. Sci.* **97**, 3171–3176.

Kalinowski, R., Dittrich, B., Hübschle, ch., Paulmann, C. & Luger, P. (2007). *Acta Cryst.* Accepted for publication.

Koritsanszky, T. (2006). *Hydrogen Bonding – New Insights*, edited by S. J. Grabowksi, pp. 441–470. Springer, Berlin.

Koritsanszky, T., Volkov, A. & Coppens, P. (2002). *Acta Cryst.* A**58**, 464–472.

Lecomte, C. (1995). *Advances in Molecular Structure Research*, Vol. 1, edited by I. Hargittai & M. Hargittai, pp. 261–302. Greenwich: JAI Press Inc.

Lecomte, C., Guillot, B., Muzet, N., Pichon-Pesme, V. & Jelsch C. (2004). *Cell. Mol. Life Sci.* **61**, 774–782.

Li, X., Wu, G., Abramov, Y. A., Volkov, A. V. & Coppens, P. (2002). *Proc. Natl. Acad. Sci.* **99**, 12132–12137.

Luger, P., Messerschmidt, M., Scheins, S. & Wagner, A. (2004). *Acta Cryst.* A**60**, 390–396.

Luger, P., Wagner, W., Hübschle, C. B. & Troyanov, S. I. (2005). *J. Phys. Chem. A*, **109**, 10177–10179.

Madsen, A. O., Sorensen, H. O., Flensburg, C., Stewart, R. F. & Larsen, S. (2004). *Acta Cryst.* A**60**, 550–561.

Palatinus, L. & van Smaalen, S. (2002). *Acta Cryst.* A**58**, 559–567.

Palatinus, L. & van Smaalen, S. (2005). *Acta Cryst.* A**61**, 363–372.

Papoular, R. J., Collin, G., Colson, D. & Viallet, V. (2002). *Proceedings of the 21st Workshop on Bayesian Inference and Maximum Entropy Methods in Science and Engineering*, edited by B. Fry. Melville, NY: American Institute of Physics.

Petricek, V., Dusek, M. & Palatinus, L. (2006). *JANA*2000. Institute of Physics, Praha, Czech Republic.

Rödel, E., Messerschmidt, M., Dittrich, B. & Luger, P. (2006). *Org. Biomol. Chem.* **4**, 475–481.

Roversi, P., Irwin, J. J. & Bricogne, G. (1998). *Acta Cryst.* A**54**, 971–996.

Roversi, P., Irwin, J. J. & Bricogne, G. (2002). *Electron, Spin and Momentum Densities and Chemical Reactivity*, edited by P. G. Mezey & B. E. Roberston. Dordrecht: Kluwer Academic Publishers.

Sakata, M. & Sato, M. (1990). *Acta Cryst.* A**46**, 263–270.
Skilling, J. (1989). *In Maximum Entropy and Bayesian Methods*, edited by J. Skilling, pp. 45–52. Kluwer Academic Publishers.
Smaalen, S. van, Palatinus, L. & Schneider, M. (2003). *Acta Cryst.* A**59**, 459–469.
Steiner, T. & Saenger, W. (1993). *Acta Cryst.* A**49**, 379–384.
Volkov, A., Abramov, Y., Coppens, P. & Gatti, C. (2000). *Acta Cryst.* A**56**, 332–339.
Volkov, A., Gatti, C., Abramov, Yu. & Coppens, P. (2000). *Acta Cryst.* A**56**, 252–258.
Volkov, A., Messerschmidt, M. & Coppens, P. (2007). *Acta Cryst.* D**63**, 160–170.
Vries, R. Y. de, Briels, W. J. & Feil, D. (1994). *Acta Cryst.* A**50**, 383–391.
Vries, R. Y. de, Briels, W. J. & Feil, D. (1996). *Phys. Rev. Lett.* **77**, 1719–1722.